Search for metal hydrides with short hydrogen–hydrogen separation: *Ab initio* calculations

P. Vajeeston,* P. Ravindran, H. Fjellvåg, and A. Kjekshus
Department of Chemistry, University of Oslo, Box 1033 Blindern, N-0315 Oslo, Norway
(Received 7 August 2003; revised manuscript received 24 March 2004; published 21 July 2004)

The present investigation is a part of a series on metal hydrides with extraordinary short H—H separations. The electronic structure, chemical bonding, and ground state properties of *RT*In (*R*=La, Ce, Pr, Nd; *T*=Ni, Pd, Pt) and their saturated hydrides $R_3T_3In_3H_4$ (=3*RT*$InH_{1.333}$) are systematically studied using the full-potential linear muffin-tin-orbital method. The effect of the metal matrix on the H—H separation in *RT*$InH_{1.333}$ is analyzed in terms of chemical bonding, and bond strength is quantitatively analyzed using the crystal-orbital-Hamilton population. Force and volume optimizations reveal that all these hydrides violate the "2-Å rule." The insertion of hydrogen in the metal matrix causes highly anisotropic lattice changes; a large expansion along *c* and a small contraction in the *a* direction. Among the 12 studied hydrides the hypothetical $LaPtInH_{1.333}$ phase exhibits the shortest H—H separation (1.454 Å). The optimized unit-cell parameters and atomic coordinates fit very well with the experimental findings for *R*$NiInH_{1.333}$, *R*=La, Ce, and Nd. Examination of the effect of the metal matrix on the H—H separation in *RT*$InH_{1.333}$ suggests that on a proper choice of alloying element one may be able to reduce the H—H separation below 1.45 Å. The H—H separation is reduced significantly by application of pressure.

DOI: 10.1103/PhysRevB.70.014107 PACS number(s): 81.05.Je, 71.15.Nc, 71.20.−b

I. INTRODUCTION

The present series of papers[1,2] concerns metal hydrides with extraordinary short H—H separations. The reversible storage of hydrogen in the form of intermetallic hydrides has several advantages over storing as gaseous and liquid hydrogen.[3,4] However, major a disadvantage of hydrides as storage media over other options is the considerable weight of the metal matrices and their relatively high cost. Hence, it seems desirable to investigate other materials for such applications at affordable cost, sufficient storage capacity, and functional reliability. Although accounting for structures and properties of prospective hydrogen storage materials still offers a tremendous challenge to improve the amount of stored hydrogen, the last two decades have seen considerable progress in the understanding of the basic problems. With the development of advanced theoretical tools, the gathering of knowledge from fields that tended to ignore each other in the past, and the progress in computer technology, one can make reliable predictions of properties for even quite complex materials.[5]

Numerous studies have been carried out to explain observed stabilities, stoichiometries, and preferred hydrogen sites in various kinds of hydrides.[6,7] It has been suggested that limiting factors in terms of minimum hole size (0.40 Å) and H—H distance (2.1 Å) in stable hydrides should be prime selection criteria for guidance about hydrogen absorption capacity.[7–10] Hence, reduction in H—H separation may be one means to enhance the hydrogen content at minimum matrix volume and mass. From experimental and theoretical studies it has been established that the separation between hydrogen atoms in interstitial matrix sites is ruled by repulsive H-to-H interactions, which in practice is assumed to prevent the hydrogen atoms to approach one another closer than 2.1 Å (Switendick's criterion).[7,9,10] Nuclear magnetic resonance (NMR) study on $CeNiInH_x$ (x=1 to 1.62)[11,12] and $PrNiInH_{1.29}$[13] has revealed that the H—H separation in these alloys is between ~1.5 and 1.8 Å. It has been suggested that both the 4*h* and 6*i* interstitial sites or either of them are occupied by hydrogen atoms in a ZrNiAl-type matrix. Although $PrNiInH_{1.29}$ has been obtained as a stable phase, no detailed structural examination has so far been reported. A recent low-temperature neutron diffraction study[14] gives evidence that H atoms occupy only the 4*h* site in an ordered arrangement in the ZrNiAl-type structure of $R_3Ni_3In_3H_4$ (=3*R*$NiInH_{1.333}$; *R*=La, Ce, and Nd hereafter referred to with the latter simple matrix-based formula) with a H—H separation of ~1.6 Å. En passant it may be mentioned that in some disordered hydrides (like K_2ReH_9[9,15]), due to the partial occupancy of the hydrogen sites, the H—H separation becomes appreciably lower than 2.1 Å.

In previous works[1,2] on *R*NiIn and *R*$NiInH_{1.333}$ (*R*=La, Ce, Nd) the origin of the anisotropic volume expansion on hydrogenation has been explained, and the presence of strong interaction between the transition metal (*T*) and hydrogen in *R*$NiInH_{1.333}$ is shown to prohibit the electrons at the hydrogen atoms from participation in repulsive interaction between two such arranged H atoms (see Fig. 1 and for more details Refs. 1 and 2). Moreover, also the *R*—*R* bond grid contributes to the shielding of the repulsive interaction between the H atoms. These observations have motivated us to search for new hydrides with short H—H separation in *RT*In matrices and in particular to identify the effect of isoelectronic substitution of Ni by Pd and Pt. In the present contribution we consider the crystal and electronic structures of nine other members of the series (*R*=La, Ce, Pr, Nd; *T*=Pd, Pt; plus $PrNiInH_{1.333}$) in addition to the earlier reported combinations with *T*=Ni, viz. all together 12 phases. Furthermore the influence on the H—H separation by application of high external pressures is considered.

The rest of this paper is organized as follows. Section II gives appropriate details about the computational methods,

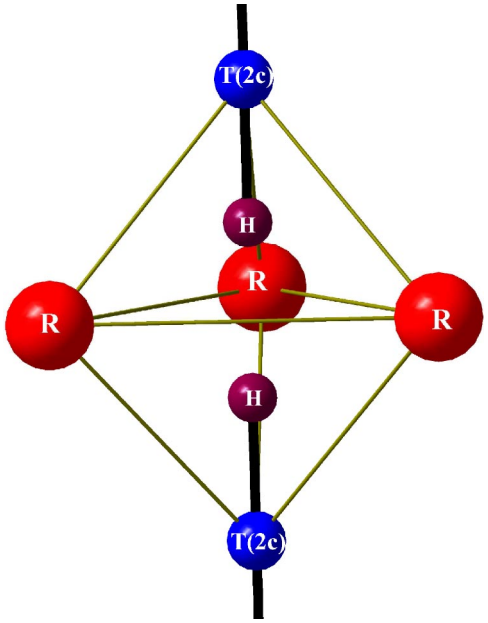

FIG. 1. (Color online) Structural fragment of $RT\mathrm{InH}_{1.333}$ (R =La, Ce, Pr, Nd; T=Ni, Pd, Pt), showing the trigonal bipyramidal coordination of 3 R and 2 $T(2c)$ around 2 H atoms. Legends to the different kinds of atoms are given on the illustration. The completion of the linear H—$T(2c)$—H units is indicated at the top and bottom of the illustration.

structural results of the calculations are presented and discussed in Sec. III, the nature of chemical bonding is analyzed in Sec. IV, and the conclusions are summarized in Sec. V.

II. DETAILS OF THE CALCULATIONS

We have used the full-potential linear muffin-tin-orbital (FPLMTO) method[16] within the generalized-gradient approximation (GGA),[17] in which the Kohn-Sham equations are solved for a general potential without any shape approximation. For the local density approximation (LDA) calculations, we have used the exchange-correlation function proposed by Hedin and Lundqvist,[18] which allows accurate calculation of the total energy as a function of volume. The unit cell is divided into nonoverlapping muffin-tin spheres, inside which the basis functions were expanded in spherical harmonics up to a cutoff in angular momentum at $\ell=6$. The basis functions in the interstitial region (i.e., outside the muffin-tin spheres) are Neumann or Hankel functions depending upon the kinetic energy. The ratio of interstitial to unit-cell volume is around 0.42. The basis set contained semicore 5p and valence 5d, 6s, 6p, and 4f states for La. For Ce, Pr, and Nd, the 4f electrons are treated as localized core electrons. In rare earth compounds, the equilibrium volume strongly depends on the valence of the f-electron-carrying element. For the present series of compounds this is a point of concern for the Ce-containing compounds. In the earlier communication[2] it is shown that only when one assumes Ce in the 3+ state in CeNiIn and $\mathrm{CeNiInH}_{1.333}$ agreement is obtained between the calculated equilibrium cell volume and the experimental cell volume. Hence, for the rest of the Ce-containing compounds in the series it was simply assumed that the valence state is Ce^{3+}. The open core approximation was used and hence contributions of the 4f electrons to the valence band are removed. This is equivalent to the LDA $+U$ approach with $U=\infty$ for the f electrons (successfully used in Ref. 19). 4s, 4p, and 3d orbitals were used for Ni; 5s, 5p, and 5d for In; semicore 4p and valence 5s, 5p, and 4d for Pd; and semicore 5p, valence 6s, 6p, and 5d for Pt; and 1s, 2p, and 3d for H. All orbitals were contained in the same energy panel. A so-called multibasis was included to ensure a well-converged wave function, implying the use of different Hankel or Neuman functions each attaching to their radial functions. This is important in order to obtain a reliable description of the higher-lying unoccupied states and low-lying semicore states. Integration over the Brillouin zone (BZ) was done using "special-point" sampling,[20,21] and self-consistency was obtained with 105 **k** points in the irreducible part of the BZ, which corresponds to 768 **k** points in the whole BZ. Test calculations were made for a doubled number of **k** points to check for convergence, but the optimized c/a ratio for 105 and 210 **k** points for $\mathrm{LaNiInH}_{1.333}$ turned out essentially the same. Hence, 105 **k** points were used consistently for the optimization of c/a, unit-cell volume, and atomic positions as well as for calculations of electron density. For the density of states (DOS) calculations, the BZ integration was performed by means of the tetrahedron method.[22]

Equilibrium volumes and bulk moduli were extracted from the calculated energy versus volume data by fitting to the "universal equation of state" proposed by Vinet *et al.*[23] Virtually the same results were obtained by fitting to the Birch[24] or Murnaghan[25] equations. For the calculation of the bulk modulus, the theoretically estimated c/a value was kept constant.

To calculate electron-localization-function plots we used the first-principles self-consistent, tight-binding, linear muffin-tin orbital (TB-LMTO) method of Andersen and Jepsen.[26] The von Barth–Hedin[27] parameterization is used for the exchange correlation potential within the local-density approximation. In the present calculation, we used the atomic sphere approximation. The calculations are semirelativistic (i.e., without spin-orbit coupling, but all other relativistic effects included) taking also into account combined correction terms. The BZ **k**-point integrations are made using the tetrahedron method on a grid of 403 **k** points in the irreducible part of BZ. In order to get more insight into the chemical bonding, we have also calculated the crystal-orbital-Hamiltonian population (COHP)[28,29] in addition to the regular band structure. The COHP is the DOS weighted by the corresponding Hamiltonian matrix elements, a positive sign of which indicating bonding character and negative antibonding character. The detailed mathematical expressions for the COHP are, e.g., found in Ref. 28. The electron-localization function (ELF) was calculated according to the TB-LMTO code.

A. Structural details

The hydrogen storage capacity of an alloy is limited in the first place by the number of interstial sites in the host lattice.

Often there exist different interstitial sites which can be occupied by hydrogen (note: as atomic H not as molecular H_2), e.g., tetrahedral and octahedral. However, owing to electrostatic limitations, most of the interstitial sites remain unoccupied on hydrogenation, and consequently the formulae for such hydrides usually take noninteger indices for the hydrogen content.[30] The ZrNiAl-type structure (space group $P\bar{6}2m$) is common among the *ABC* intermetallics, more than 300 examples being recorded.[31] In the *RT*In lattice the most favorable sites for the hydrogen have tetrahedral surroundings: (a) 6*i* at x, 0, z etc. ($x \approx 0.25$, $z \approx 1/3$), coordinated by three *R*s and one In; (b) 4*h* at $1/3$, $2/3$, x etc. ($x \approx 2/3$), coordinated by three *R*s and one *T*(2*c*) (illustrated in Fig. 1); and (c) 12*l* at x, y, z etc. ($x \approx 0.44$, $y \approx 0.16$, $z \approx 2/9$), coordinated by two *R*s, one In, and one *T*(1*b*). The shortest 4*h*–4*h* and 6*i*–6*i* separations occur along the *c* axis of the hexagonal structure. Recent experimental findings show that H prefer only the 4*h* among the available sites.[14] However, the complete filling of such arranged tetrahedral sites with hydrogen has been considered unlikely on the basis of the requirements of the hole size and the "2-Å rule".[32] All calculations reported here assume ideal and fully saturated hydrides with the formula $3RTInH_{1.333}$.

III. STRUCTURAL ASPECTS

In order to understand the role of the *R* and *T* components in the *RT*In metal matrix for the unusual H—H separation and the anisotropic volume expansion on hydrogenation a structural optimization study has been carried out. The ZrNiAl-type structure with the experimental lattice parameters and atomic positions for the appropriate compounds[14] were chosen as the starting point. First all variable atom coordinates were relaxed globally (by keeping c/a and cell volume constant) using the force minimization technique. The atomic coordinates were then fixed at their optimized values while the unit-cell volume were varied in steps of 5% within ±15% from the optimized value. The thus obtained total energy versus unit-cell volume curve was fitted to a polynomial and the minimum, which represents the theoretical equilibrium volume, was established. The theoretical c/a was, in turn, determined from the minimum in total energy versus c/a at fixed atomic coordinates and equilibrium unit-cell volume. Finally, once again we relaxed the atom coordinates globally by fixing c/a and unit-cell volume. The thus obtained atomic coordinates differ less than 1% from the first established values. The calculated data are in good agreement with the experimental findings (see Tables I and II). The next step was to introduce the hydrogen atoms in the 4*h* position of the optimized metal matrix. This results in local strain, which implies that the entire, just-outlined, structural optimization process had to be repeated. The then obtained atomic coordinates and unit-cell dimensions agree very well (see Tables I and II) with recent powder neutron diffraction findings for the phases with *T*=Ni.[14] The lattice changes during the hydrogenation are highly anisotropic, on the average 16% expansion along *c* and a small contraction (average ~2.5%) along *a*, the largest anisotropy being found within the *T*=Pd series.

On going from La to Nd the calculated unit-cell volume decreases gradually, a trend that is recognized also in the experimental data (see Fig. 2). A similar trend was observed by Muller, Blackledge, and Libowitz[34] in RH_2 phases, which in that case, was attributed to the lanthanide contraction. Experimentally all intermetallic mother phases except CePtIn have been identified,[14,31] whereas most of the hydrogenated phases are yet structurally little explored (see Tables I and II).

In order to check possible effects of different computational approaches we have performed structural optimizations for the $RPtInH_{1.333}$ phases [among which the shortest H—H separations are found] using both LDA and GGA exchange correlation functionals (see Table III). Due to the overestimation of bond characteristics by LDA the calculated H—H seprations come out smaller by this approach than those obtained by GGA. For rest of the compounds we only used the GGA formalism and the following discussion is solely based on the GGA calculations.

The calculated unit-cell volume versus total energy is fitted to the "universal equation of state" in order to estimate the bulk modulus (B_0) and its pressure derivative (B_0') for these *RT*In and $RTInH_{1.333}$ phases (see Table IV). On going from the *R*NiIn mother phases to the corresponding hydrides, B_0 is reduced (except for NdNiIn), which can be understood as a consequence of the volume expansion during hydrogenation. On the other hand, on going from the *R*PdIn and *R*PtIn series to their hydrides, B_0 increases (except for LaPtIn). This may be due to enhanced bond strength in the *RT*In matrix (in an extent that overcomes the volume expansion effect) on introduction of the hydrogen. No experimental data for B_0 of these compounds are available.

IV. CHEMICAL BONDING

A. DOS

From the characteristic features of the DOS, one may be able to rationalize (see, e.g., Ref. 35) the bonding in the *RT*In series and changes introduced in the bonding upon the hydrogenation. No electronic structure calculations have apparently hitherto been undertaken for *RT*In phases. In general all members of the *RT*In and $RTInH_{1.333}$ series (see Table IV) have a finite number of electrons at the Fermi level (E_F), which classifies them as metals. As examples the DOS for LaPtIn and $LaPtInH_{1.333}$ is shown in Fig. 3. For LaPtIn it is convenient to divide the DOS into regions: region I (−8 to −5 eV) with well localized In-*s* and Pt-*s* states and some hybridized La-*s* states; region II (−5 eV to E_F) with hybridized In-*p*, Pt-*d*, and La-*d* states; and region III (above E_F) with unoccupied states. By studying the changes in these regions on hydrogenation one can extract valuable information about the changes in bonding character upon hydrogenation. Region II where the In-*p*, Pt-*d*, and La-*d* states are energetically degenerate, signals an appreciable degree of covalent bonding. The electronegativity (Pauling scale) differences between In and Pt (0.5) and In and La (0.6) are much smaller than between La and Pt (1.1), which indicate that the tendency to form covalent bonding between the former pairs

TABLE I. Calculated a,c (in Å), and c/a for RTIn and $RT\mathrm{InH}_{1.333}$; and changes $\Delta a/a$, $\Delta c/c$, and $\Delta V/V$ (in %) on hydrogenation.

	a		c		c/a		$\Delta a/a$		$\Delta c/c$		$\Delta V/V$	
Compound	Theor.	Expt.	Theor.	Expt.	Theor.	Expt.	Theor.	Expt.	Theor.	Expt.	Theor.	Expt.
LaNiIn	7.5604	7.5905[a]	3.9924	4.05000[a]	0.5281	0.5336[a]	-	-	-	-	-	-
$LaNiInH_{1.333}$	7.3771	7.3810[a]	4.6254	4.6489[a]	0.6270	0.6399[a]	−2.43	−2.76	15.86	14.80	10.31	8.54
LaPdIn	7.7716	7.7290[b]	4.1250	4.1330[b]	0.5307	0.5347[b]	-	-	-	-	-	-
$LaPdInH_{1.333}$	7.3501	-	4.8112	-	0.6546	-	−5.42	-	16.64	-	4.33	-
LaPtIn	7.7277	7.6950[b]	4.1144	4.1250[b]	0.5324	0.5361[b]	-	-	-	-	-	-
$LaPtInH_{1.333}$ (LDA)	7.5262	-	4.6261	-	0.6147	-	−2.44	-	12.44	-	6.65	-
$LaPtInH_{1.333}$ (GGA)	7.7274	-	4.6903	-	0.6070	-	−0.04	-	13.98	-	14.00	-
CeNiIn	7.5807	7.5340[a]	3.9806	3.9750[a]	0.5251	0.5276[a]		-	-	-	-	-
$CeNiInH_{1.333}$	7.4536	7.2921[a]	4.4871	4.6238[a]	0.6020	0.6341[a]	−1.68	−3.21	12.72	16.3	8.97	8.98
CePdIn	7.8113	7.7290[b]	4.1257	4.1330[b]	0.5282	0.5347[b]	-	-	-	-	-	-
$CePdInH_{1.333}$	7.4494	-	4.8676	-	0.6534	-	−4.63	-	17.98	-	7.30	-
CePtIn	8.0112	-	3.9800	-	0.4892	-	-	-	-	-	-	-
$CePtInH_{1.333}$ (LDA)	7.6419	-	4.6467	-	0.6081	-	−4.61	-	16.75	-	6.24	-
$CePtInH_{1.333}$ (GGA)	7.8250	-	4.7101	-	0.6019	-	−2.32	-	18.34	-	12.098	-
PrNiIn	7.5950	7.5410[b]	3.9259	3.9500[b]	0.5149	0.5238[b]	-	-	-	-	-	-
$PrNiInH_{1.333}$	7.3783	7.2600[c]	4.4726	4.5600[c]	0.6062	0.6281[c]	−2.85	−3.73	13.93	15.40	7.52	7.01
PrPdIn	7.8674	7.3790[b]	4.0257	4.0430[b]	0.5117	0.5265[b]	-	-	-	-	-	-
$PrPdInH_{1.333}$	7.4107	-	4.8041	-	0.6483	-	−5.81	-	19.34	-	5.88	-
PrPtIn	7.8042	7.6522[b]	4.0706	4.0455[b]	0.5216	0.5287[b]	-	-	-	-	-	-
$PrPtInH_{1.333}$ (LDA)	7.5766	-	4.6283	-	0.6109	-	−2.92	-	13.70	-	6.69	-
$PrPtInH_{1.333}$ (GGA)	7.7595	-	4.6934	-	0.6049	-	−0.06	-	15.30	-	13.98	-
NdNiIn	7.5207	7.5202[a]	3.9023	3.9278[a]	0.5189	0.5223[a]	-	-	-	-	-	-
$NdNiInH_{1.333}$	7.2408	7.2255[a]	4.5560	4.5752[a]	0.6292	0.6332[a]	−3.72	−3.92	16.75	16.50	7.60	7.53
NdPdIn	7.7898	7.6830[b]	3.9735	3.9970[b]	0.5101	0.5202[b]	-	-	-	-	-	-
$NdPdInH_{1.333}$	7.3519	-	4.7895	-	0.64515	-	−5.62	-	20.54	-	7.37	-
NdPtIn	7.7610	7.6360[b]	3.9815	4.0100[b]	0.5130	0.5251[b]	-	-	-	-	-	-
$NdPtInH_{1.333}$ (LDA)	7.5362	-	4.6172	-	0.6127	-	−2.90	-	15.97	-	6.35	-
$NdPtInH_{1.333}$ (GGA)	7.6980	-	4.6750	-	0.6073	-	−0.08	-	17.40	-	15.52	-

[a]Ref. 14
[b]Ref. 31
[c]Ref. 13

of elements is more favorable than that between La and Pt. Indium is surrounded by four transition-metal atoms (two in 2*c* and another two in 1*b* site) and six rare-earth atoms. Owing to the crystal field splitting the In-*p* state separates into two parts (see the partial DOS of In in Fig. 4) between −5 to −2.5 eV the p_z electrons mainly dominate whereas the non-bonding p_x and p_y electrons reside at the top of the valence band (VB). It is the well-separated p_z states that participate in the covalent bonding with the energetically nearest Pt-*d* states.

Figure 3 shows that when hydrogen is inserted in the LaPtIn matrix, new states are formed around −9.5 to −2.5 eV. Hence the VB is shifted to lower energy and the E_F is pushed slightly upward. It is commonly accepted that on insertion of hydrogen in a metal matrix, the hydrogen will absorb some valence electrons from the nearest electron-rich metal atom(s), viz. a charge-transfer effect. In the $RT\mathrm{InH}_{1.333}$ series H absorbs electrons from all the metal atoms of the mother matrix (see Sec. IV B). In general, the so-called core-level shifts observed in photo-electron spectra during formation of metal hydrides[36] may be regarded as direct evidence of charge transfer from metal atoms to the hydrogens. In the LaPtIn-to-$LaPtInH_{1.333}$ case, the La-5*p* level is lowered by ~0.8 eV; (present at around −17 eV; not shown in Fig. 4); similar shifts being reported[37] in rare-earth hydrides. The detailed features of the partial Pt DOS for $T(1b)$ and $T(2c)$ show some distinction due to their different atomic environments. The total width of the VB is lower in LaPtIn than $LaPtInH_{1.333}$ (similar for the other pairs of compounds studied). This is due to the fact that hydrogen enhances the interaction between neighboring atoms, and thereby increases the overlap of the orbitals concerned. Further, the location of the H-*s* state at the bottom of the VB also contributes to an increase in the width of the VB. In particular the contribution of Pt($2c$) to the VB enhances the width from 8 to 9.5 eV, whereas contributions of Pt($1b$) and In on the other hand,

TABLE II. Optimized atomic coordinates for *RT*In and $RTInH_{1.333}$ phases.[a]

	*RT*In		*RT*$InH_{1.333}$			
	Theor. *x*	Expt. *x*	Theor. *x*	Expt. *x*	Theor. *z*	Expt. *z*
T=Ni						
R=La	0.5866	0.594	0.6036	0.6035	1/2	1/2
In	0.2475	0.256	0.2444	0.2437	0	0
H			1/3	1/3	0.6728	0.6759
R=Ce	0.588	0.594	0.6077	0.6013	1/2	1/2
In	0.248	0.256	0.2507	0.2462	0	0
H			1/3	1/3	0.6752	0.6737
R=Pr	0.585	0.594	0.6059		1/2	1/2
In	0.248	0.256	0.2568		0	0
H			1/3	1/3	0.6663	
R=Nd	0.5886	0.594	0.6013	0.6013	1/2	1/2
In	0.2496	0.256	0.2483	0.2462	0	0
H			1/3	1/3	0.6723	0.6737
T=Pd						
R=La	0.5930	0.594	0.6008		1/2	
In	0.2537	0.256	0.2441		0	
H			1/3		0.6583	
R=Ce	0.5885		0.6055		1/2	
In	0.2501		0.2517		0	
H			1/3		0.6636	
R=Pr	0.5895	0.594	0.6015		1/2	
H			1/3		0.6663	
R=Pr	0.5895	0.594	0.6015		1/2	
In	0.2529	0.256	0.2440		0	
H			1/3		0.6624	
R=Nd	0.5913	0.594	0.60414		1/2	
In	0.2535	0.256	0.2695		0	
H			1/3		0.65045	
T=Pt						
R=La	0.5874	0.594	0.6020		1/2	
In	0.2533	0.256	0.2460		0	
H			1/3		0.6551	
R=Ce	0.5908	0.594	0.6061		1/2	
In	0.2525	0.256	0.2456		0	
H			1/3		0.6554	
R=Pr	0.5894	0.594	0.6034		1/2	
In	0.2516	0.256	0.2486		0	
H			1/3		0.6595	
R=Nd	0.5904	0.594	0.6035		1/2	
In	0.2548	0.256	0.2513		0	
H			1/3		0.6639	

[a]*R* in $3g(x,0,1/2)$, *T*(1*b*) in $1b(0,0,1/2)$, *T*(2*c*) in $2c(1/3,2/3,0)$, In in $3f(x,0,0)$, and H in $4h(1/3,2/3,z)$.

would have reduced the width of the VB from ~8 to 7.5 eV. The latter modification reflects the increase in the Pt(1*b*)—In separation following from the insertion of the additional H atoms between the Pt(2*c*)–Pt(2*c*) linear configuration.[2]

The interatomic Pt(2*c*)—H distance almost equals the sum of the covalent radii of Pt and H (not only in $LaPtInH_{1.333}$, but also in the rest of the compounds). The H-*s*, In-*s*, and Pt(2*c*)-*d* electrons are energetically degenerate in the energy range between −9.75 and −2.50 eV. According to the electronegativity differences of 0.0, 0.5, and 1.2 for Pt—H, In—H, and La—H, respectively, covalent bonding between Pt and H is more likely than between La and H. Careful inspection of the partial DOS of Pt(2*c*) and H in Fig.

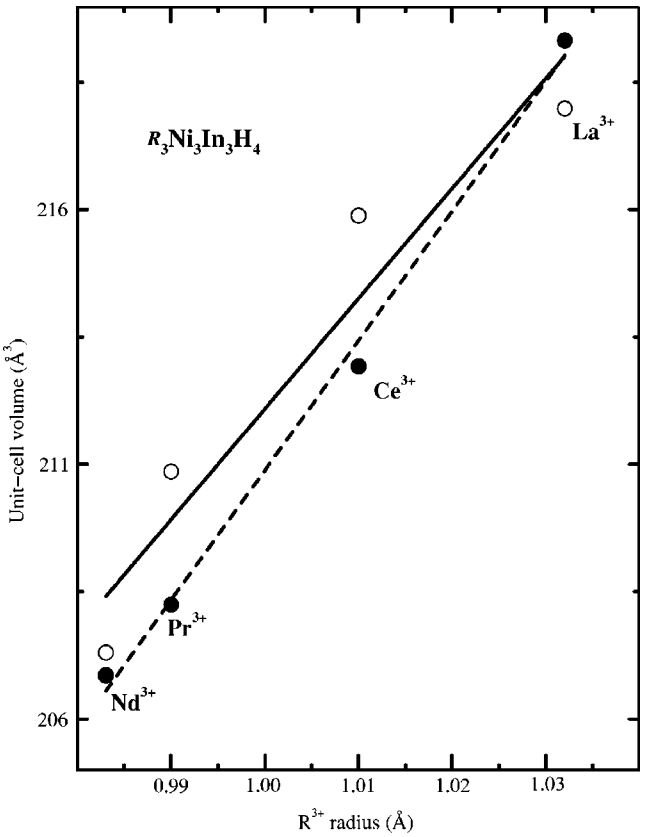

FIG. 2. Experimental (●) and calculated (○) unit-cell volume for $R_3Ni_3In_3H_4$ versus ionic radius[33]. Experimental data for $PrNiInH_{1.29}$ from Ref. 13 and for the other phases from Ref. 14.

4 shows accumulation of *d* electrons in the range −4.25 to −1 eV, whereas most of the H electrons are localized in the range −9.75 to −2.35 eV, indicating that the interaction between H and Pt is far from perfect covalent.

B. Charge density and charge transfer

The unusually short H—H separations in the *RT*$InH_{1.333}$ phases (Table III) are a motivation for further penetration into the nature of their bonding. The variation in the electron distribution on replacement of *R* or *T* components may be expected to give hints about factors which influence the bonding between the H atoms as well as between H and *T*.

1. Charge density

The charge-density contours in the (100) plane of LaPtIn and $LaPtInH_{1.333}$ are displayed in Figs. 5 and 6(a), respectively. Owing to the pronounced mutual similarities between the charge density within the *RT*In and *RT*$InH_{1.333}$ series we present only illustrations for the charge density of LaPtIn and $LaPtInH_{1.333}$ (Figs. 5 and 6), the latter hydride having moreover the shortest H—H separation among the investigated hydrides. The finite electron distribution present between Pt(2*c*) and In (Fig. 5) clearly indicates that the interaction between these atoms has an appreciable covalent component. The *R*—Pt(1*b*) and *R*—In bonds have mixed (partial covalent and partial ionic) character also suggested by their different electronegativities.

In order to gain insight in the impact on the bonding interaction between metal atoms of the mother matrix upon hydrogenation Fig. 6(a) shows the charge density for $LaPtInH_{1.333}$. The interesting aspect is that, the charge density of Pt(2*c*) is directed toward H, leading to the formation of dumb-bell shaped H—Pt(2*c*)—H units, linked like a chain along [001]. The interatomic separation between Pt(2*c*) and H in $LaPtInH_{1.333}$ corresponds nearly to the sum of the covalent radii of Pt and H. The same trend (viz. very short *T*—H separations) is observed in all the studied phases. The H-1*s* electrons participate in pairing mediated via Pt(2*c*) to a molecule-like structural (H—Pt—H) unit as well as in H…H interactions with neighboring H—Pt—H units (viz. a linear arrangement …H—Pt—H…H—Pt—H…). Examination of the partial DOS (in Fig. 4) shows that the valence electrons of Pt and H are not fully energetic degenerate in the VB region indicating a degree of ionic character in the Pt-to-H bonding. This interpretation is supported by the charge-transfer map [Fig. 6(b)]. The bond strength of Pt(2*c*)—In is reduced upon hydrogenation as reflected in the increased interatomic distance from 2.93 to 2.97 Å, and further confirmed by the COHP analyses. An important difference between the complex hydrides and the present type of hydrides lies in the nature of the interaction between the H atoms. Most of the complex hydrides have nonmetallic character, for example, in $LiAlH_4$ there is strong covalent interaction between Al and H (within the AlH_4 subunits) and very weak H—H bonds between two AlH_4 subunits.[38] In *RT*$InH_{1.333}$, on the other hand, there is a finite electron density distributed between the TH_2 subunits implying a considerable H—H interaction.

2. Charge transfer plot

A convenient and illustrative way to represent and analyze the bonding effects in the *RT*$InH_{1.333}$ series is to use charge-transfer plots. The charge-transfer contour is the self-consistent electron density in a particular plane, $\rho_{comp.}$, minus the electron density of the overlapping free atoms, $\rho_{o.f.a.}$, i.e.,

$$\Delta\rho(r) = \rho(r)_{comp.} - \rho(r)_{o.f.a.}, \quad (1)$$

which allows one to visualize how electrons are redistributed in a particular plane compared to free atoms due to the bonding in the compound.

Since the charge-transfer plots for all *RT*$InH_{1.333}$ phases show close qualitative similarity, the following considerations are limited to $LaPtInH_{1.333}$. Figure 6(b) shows that charge has been depleted from the La, Pt, and In sites and transferred to H, but the magnitude of charge transfer varies in different directions of the crystal. Most charge has been transferred from In, but not isotropically and the resulting charge distribution at the In site is certainly not spherically symmetric. There is a significant amount of extra electron density around the H atoms, and also an increased amount of electrons in the interstitial region between the Pt(2*c*) and In atoms. The charge transfer from the metal components to the H atoms leads to an appreciable ionic component in the

TABLE III. Interatomic distances (in Å), and ICOHP (in eV) for $RT\mathrm{InH}_{1.333}$ phases.

	R—H			*T*—H			H—H		
Compound	Theor.	Expt.[a]	ICOHP	Theor.	Expt.[a]	ICOHP	Theor.	Expt.[a]	ICOHP[b]
$LaNiInH_{1.333}$	2.3993	2.4064	−0.710	1.5132	1.5065	−3.211	1.5983	1.6350	−0.121
$LaPdInH_{1.333}$	2.3727	-	−0.747	1.6440	-	−2.829	1.5230	-	−0.319
$LaPtInH_{1.333}$ (LDA)	2.4018	-	−0.631	1.6167	-	−3.595	1.3923	-	−0.442
$LaPtInH_{1.333}$ (GGA)	2.4748	-	−0.642	1.6177	-	−3.539	1.4543	-	−0.423
$CeNiInH_{1.333}$	2.4271	2.3708	−0.791	1.4573	1.5086	−3.322	1.5721	1.6061	−0.224
$CePdInH_{1.333}$	2.4238	-	−0.691	1.6373	-	−2.838	1.5925	-	−0.256
$CePtInH_{1.333}$ (LDA)	2.4532	-	−0.605	1.6011	-	−3.659	1.4440	-	−0.326
$CePtInH_{1.333}$ (GGA)	2.5098	-	−0.534	1.5883	-	−3.621	1.4637	-	−0.313
$PrNiInH_{1.333}$	2.3873	-	−0.629	1.4924	-	−3.397	1.4874	-	−0.307
$PrPdInH_{1.333}$	2.3979	-	−0.668	1.6217	-	−2.895	1.5602	-	−0.281
$PrPtInH_{1.333}$ (LDA)	2.4298	-	−0.489	1.6012	-	−3.615	1.4252	-	−0.351
$PrPtInH_{1.333}$ (GGA)	2.4955	-	−0.582	1.5979	-	−3.645	1.4970	-	−0.365
$NdNiInH_{1.333}$	2.3499	2.3499	−0.690	1.4928	1.5064	−3.341	1.4928	1.5618	−0.231
$NdPdInH_{1.333}$	2.3682	-	−0.528	1.6740	-	−2.652	1.4411	-	−0.579
$NdPtInH_{1.333}$ (LDA)	2.4160	-	−0.555	1.6025	-	−3.635	1.4118	-	−0.396
$NdPtInH_{1.333}$ (GGA)	2.4817	-	−0.384	1.5711	-	−3.614	1.5323	-	−0.384

[a]From Ref. 14
[b]ICOHP value up to bonding states.

bonds to H. The charge transfer to the interstitial regions between Pt($2c$) and In reflects covalent bonding.

C. ELF

ELF is a ground-state property that discriminates between different kinds of bonding interaction for the constituents of solids.[39–41] In the implementation for density-functional theory, this quantity depends on the excess of local kinetic energy t_p originating from the Pauli principle.

$$\mathrm{ELF} = \{1 + [t_{p(r)}/t_{p,h}(\rho(r))]^2\}^{-1}, \tag{2}$$

where:

$$t_p = \tau - 1/8[(\nabla\rho)^2/\rho] \tag{3}$$

is the Pauli kinetic energy density of a closed-shell system. $(\nabla\rho)^2/(8\rho)$ is the kinetic energy density of the bosonic-like system, where orbitals proportional to $\sqrt{\rho}$ are occupied. t_p is always positive and, for an assembly of fermions, it describes the additional kinetic energy density required to satisfy the Pauli principle. The total electron density, ρ:

$$\rho = \sum_i^n |\psi_i|^2 \tag{4}$$

as well as the kinetic energy density:

$$\tau = 1/2\sum_i^n |\nabla\psi_i|^2 \tag{5}$$

are computed from the orbitals, ψ_i. In both equations, the index i runs over all occupied orbitals.

According to Eq. (2) the ELF takes the value one either for a single-electron wave function or for a two-electron singlet wave function. In a many-electron system, ELF is close to one in regions where electrons are paired in a covalent bond, or for the unpaired lone electrons of a dangling bond, while the ELF is small in low-density regions. In a homogeneous electron gas ELF equals 0.5 at any electron density, and ELF values of this order in homogeneous systems indicates regions where the bonding has a metallic character. The estimated ELF value of ca. 0.38 between the nearest neighbor hydrogens indicates metallic-like interaction. The ELF value between Pt($2c$) and H is relatively small. It is interesting to note that our test calculations for Ni, Co, and Cu metals shows that such low ELF values are generally characteristic of transition metals (d electrons). This clearly indicates that metallic Pt($2c$)-5d electrons are mainly present between Pt($2c$) and H, and hence the apparently appreciable Pt($2c$)—H bond strength (seen by the COHP analysis) originates from a metallic-like situation with additional small ionic interactions between the atoms concerned. The large

TABLE IV. Calculated ground-state properties: $N(E_F)$ (in states/Ry cell), bulk modulus B_0 (in GPa), and its pressure derivative B_0'.

Compound	$N(E_F)$	B_0	B_0'
LaNiIn	38.22	70.4	4.1
LaPdIn	39.33	74.9	4.2
LaPtIn	28.42	85.4	4.3
$LaNiInH_{1.333}$	35.30	69.5	4.1
$LaPdInH_{1.333}$	24.10	86.1	4.2
$LaPtInH_{1.333}$	37.40	77.6	4.3
CeNiIn	38.90	86.2	2.9
CePdIn	47.67	71.3	4.4
CePtIn	26.15	80.8	4.4
$CeNiInH_{1.333}$	38.10	81.7	3.5
$CePdInH_{1.333}$	30.03	84.6	4.4
$CePtInH_{1.333}$	37.56	86.4	4.3
PrNiIn	44.53	73.4	4.4
PrPdIn	42.21	74.1	4.4
PrPtIn	27.06	83.7	4.5
$PrNiInH_{1.333}$	55.58	71.1	4.0
$PrPdInH_{1.333}$	33.34	101.0	4.4
$PrPInH_{1.333}$	33.36	88.4	4.3
NdNiIn	43.74	76.0	4.4
NdPdIn	50.69	74.7	4.8
NdPtIn	27.46	86.0	4.4
$NdNiInH_{1.333}$	28.13	86.0	4.1
$NdPdInH_{1.333}$	32.88	89.7	4.5
$NdPtInH_{1.333}$	30.93	101.8	4.5

ELF value at the H site indicates the presence of largely paired electrons. Owing to the repulsive interaction between the negatively charged H electrons, the ELF contours are not spherically shaped but rather polarized toward La and In. The localized nature of the electrons at the H site and their polarization toward La and In reduce significantly the H-to-H repulsive interaction and this can explain the unusually short H—H separation in this series of compounds.

D. COHP

Implications of COHP is that a negative value indicates bonding and positive antibonding states. In order to get insight in the bond strength between two interacting atoms in a solid, one should examine the entire COHP between them,

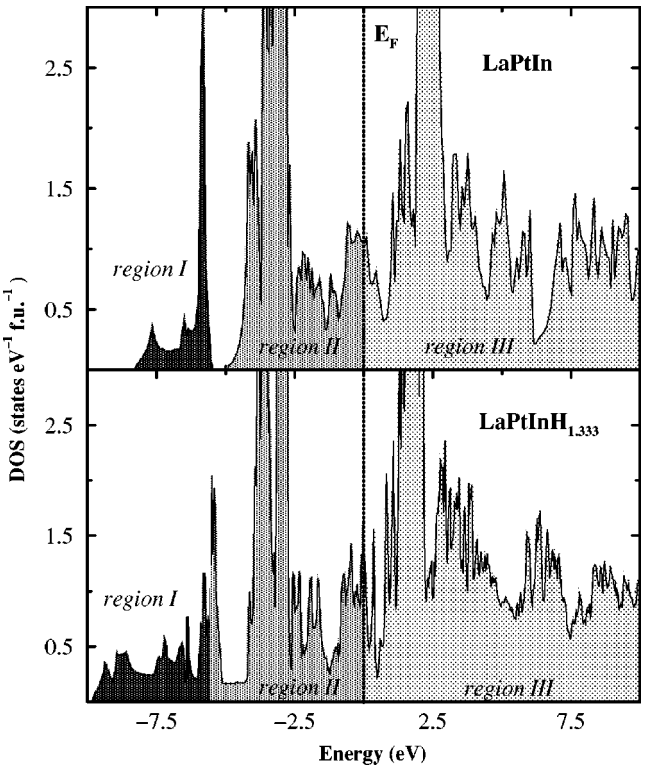

FIG. 3. Total DOS for LaPtIn (top panel) and $LaPtInH_{1.333}$ (bottom panel).

taking all valence orbitals into account.[29] The COHP contours depend on the number of states in a particular energy interval. The integrated COHP (ICOHP) curve up to the E_F is the total overlap population of the bond in question.

Figure 7 shows COHP curves of the *T*—H and H—H bonds for Pr*T*In$H_{1.333}$. When one includes hydrogen in the *RT*In matrix the estimated ICOHP value for the *T*—In bond is changed from ca. −0.8 to −1.1 eV. This appears to reflect transfer of electrons from both *T* and In to the H site, which reduces the covalent interaction between *T* and In upon hydrogenation. All *RT*In$H_{1.333}$ phases studied have short *T*—H separations (1.457 to 1.674 Å; see Table III) approaching the sum of the covalent radii of *T* and H and indicates the presence of covalent bonding. However, our charge-density, charge-transfer, and ELF analyses show that nonbonding *T*-*d* electrons are found between *T* and H, and the bonding interaction between *T* and H is dominated by the transferred charge. Another important observation is that all Ni-based phases have shorter *T*—H distances than those containing Pt and Pd (in fact the *T*—H distances follow the sequence: Ni < Pt < Pd), which is consistent with the sequence of the covalent radii of the involved elements. On comparing the estimated ICOHP values for the different combinations (like *R*—H, *R*—In, *T*(2*c*)—In, *T*(1*b*)—In, and H—H), it is seen that these combinations take a peak value at *T*(2*c*)—H, which ultimately indicates that the interaction between *T* and H is stronger than the other interactions. The charge-density, charge-transfer, and ELF analyses show that this interaction does not have a specific bonding character and indeed exhibit metallic interaction with a small ionic component. A similar type of bonding situation is reported[42] for $LaNi_5H_7$.

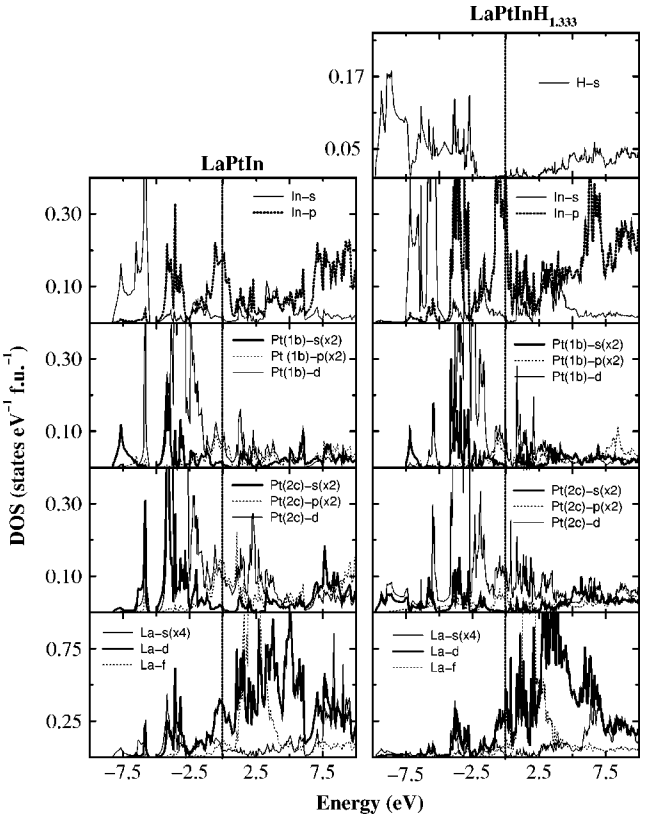

FIG. 4. Partial DOS for LaPtIn (left panel) and $LaPtInH_{1.333}$ (right panel).

The ICOHP values for the H—H separations in the $RTInH_{1.333}$ series are very small, around −0.04 eV, thus supporting the already advanced inference that there is no significant covalent bonding interaction between the H atoms (Sec. IV B 1). The low ICOHP value reflects the fact that both bonding and antibonding states are present below E_F, but even if one takes into account only the bonding states, ICOHP remains low [−0.14 to −0.23 eV, which is much smaller than the ICOHP for $T(2c)$—H]. Hence, both COHP and charge-density analyses agree that the H—H interaction is considerably weaker than the $T(2c)$—H interactions. When we compare the H—H interaction in these series, the Pt-based phases have stronger interactions (ICOHP between −0.313 to −0.423 eV) than the others (except $NdPdInH_{1.333}$).

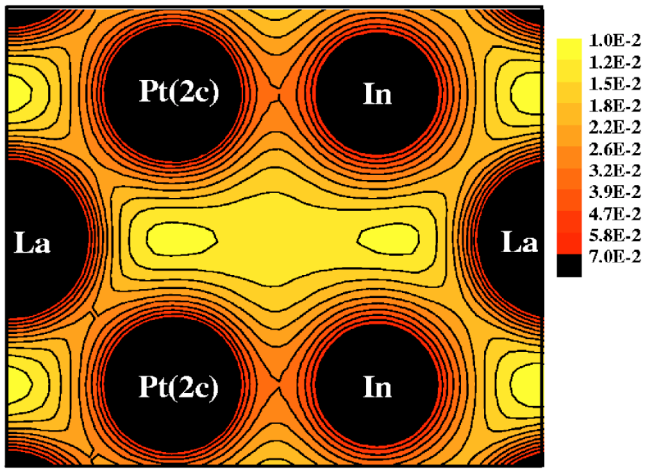

FIG. 5. (Color online) Calculated valence-electron-density map for LaPtIn in the (100) plane. (1.0E-2 is an abbreviation for 1.0×10^{-2} etc.)

E. Effect of pressure on c/a and H—H separation

In order to explore the effect of pressure on the H—H separation we have made a high-pressure study on $LaNiInH_{1.333}$ up to 400 GPa. The pressure was evaluated from the derivative of the total energy with respect to volume, i.e., calculated energy versus volume data are fitted to a universal equation of state from which the bulk modulus and its pressure derivative are calculated.[23] The calculated H—H separation and the shrinkage in a and c (viz. Δa and Δc with respect to the equilibrium values) as a function of pressure shows a considerably and nonlinear variation as a function of pressure. The H—H separation (Fig. 8) has become ca. 1.1 Å at 400 GPa. Similarly, a and c also decrease in the same manner but the magnitude of the shrinkage varies with the direction, which is in agreement with recent high-pressure experiments.[43] The difference between Δa and Δc may be classified as somewhat insignificant at lower pressure (say up to 40 GPa; $\Delta a - \Delta c = 0.16$ and 0.63 Å at 20 and 200 GPa, respectively). Because of the structural …H-Ni-H…H-Ni-H… configuration in the linear chains along c one should of course have anticipated such anisotropic lattice expansion/contraction upon application of pressure. It should be noted that a recent experimental study[43] shows there is no pressure-induced structural transition in this material up to 40 GPa. Hence, we have assumed that the ambient pressure phase will be stable at higher pressures also. The calculated total energy is increased monotonically without discontinuities and indications of local minima upon increasing pressure. This ultimately implies that formation of molecular-like H_2 units in this particular structure does not occur at least up to 400 GPa, even though the H—H separation has approached the bond distance in the H_2 molecule (0.746 Å).

F. Is the $RTInH_{1.333}$ compounds really metal hydrides?

The TH_2 structural subunit in the $RTInH_{1.333}$ compounds resembles a linear complex molecule and the adjacent subunits are also arranged in a linear fashion as often found in structures of linear complex molecules. For completely noninteracting molecules one would have anticipated that the "2-Å rule" should have been applicable, but for the present compounds this is certainly not the case. However, these compounds are not complex hydrides, for the following reasons:

1) The two H atoms within a given trigonal bipyramid (see Fig. 1) are not completely isolated from each other as would have been the case in complex hydrides.

2) In $RTNiInH_{1.333}$ there are considerable interactions between the H atoms as evidence by the fact that the H—H distance also varies considerably on displacement of the R atoms.[1,2] If the TH_2 units had been mutually completely non-

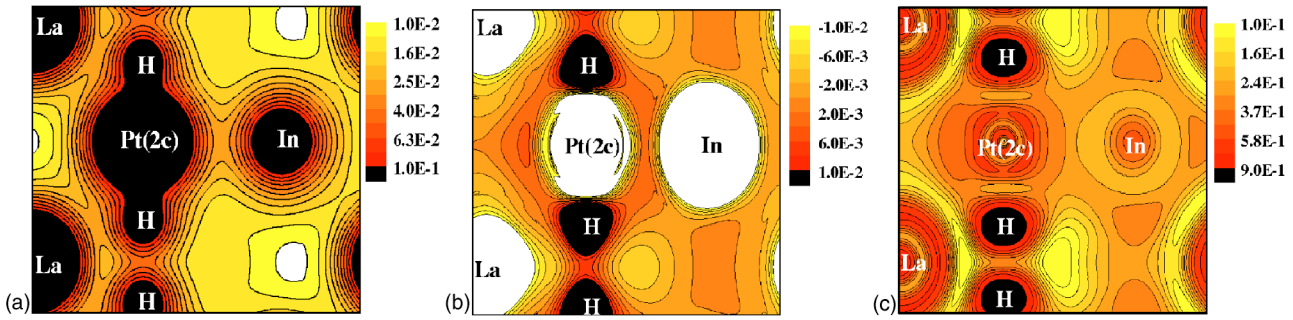

FIG. 6. (Color online) Calculated (a) valence-electron-density map, (b) charge transfer map, and (c) ELF map for $LaPtInH_{1.333}$, in (100). (1.0E-2 is an abbreviation for 1.0×10^{-2} etc.)

interacting, then the H—H distance should not have been sensitive to displacements of *R*.

3) If the $RTInH_{1.333}$ compounds should be viewed as complex hydrides[44] with isolated TH_2 molecular units, then the desorption of hydrogen from the host lattice may be expected to require high temperature. However, experimental studies show[14] that desorption of hydrogen from $RTInH_{1.333}$ takes place in a rather low-temperature range around 100 °C, viz. typical for a metal hydride.

4) In general, complex hydrides possess nonmetallic behavior,[45] but the electronic structure calculations show that $RTInH_{1.333}$ behave like metal.

5) Unlike many complex hydrides, the $RTInH_{1.333}$ series can be prepared by the traditional methods used for the synthesis of intermetallic hydrides.

6) Complex metal hydrides have molecular character with stoichiometric hydrogen contents. On the contrary, in the $RTInH_{1.333}$ phases the hydrogen content can be varied like in metal hydrides.[14,32]

7) The COHP analyses show that a considerable COHP is

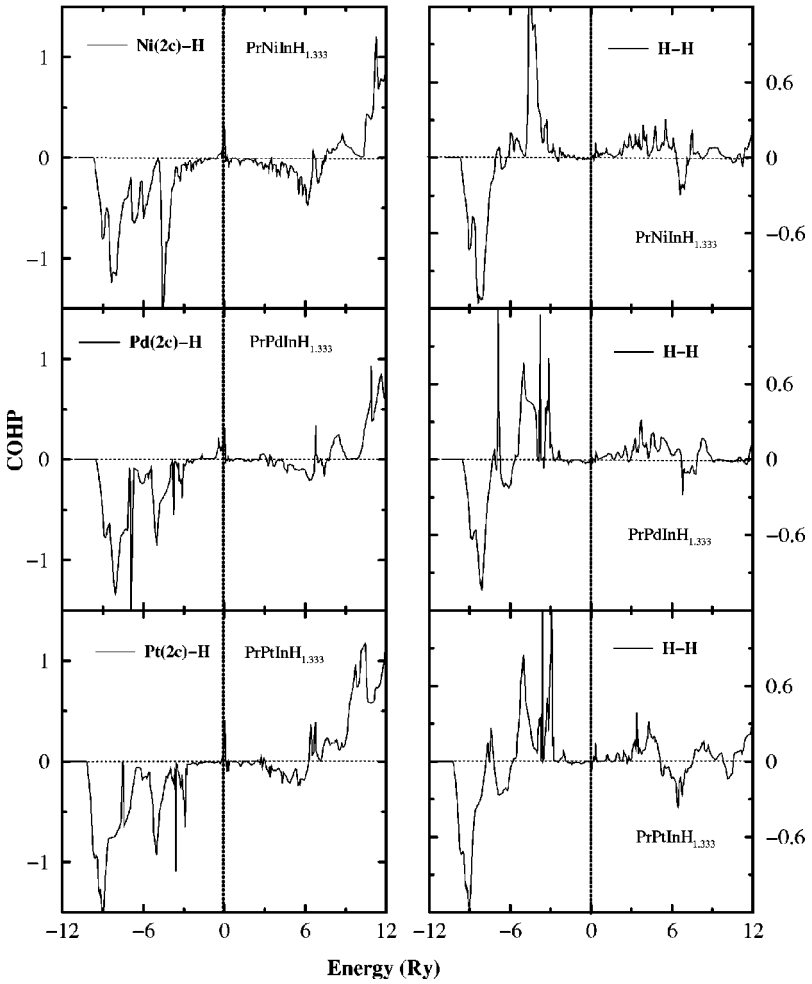

FIG. 7. COHP for $PrTInH_{1.333}$ (T=Ni, Pd, Pt) describing the T—H and H—H interactions.

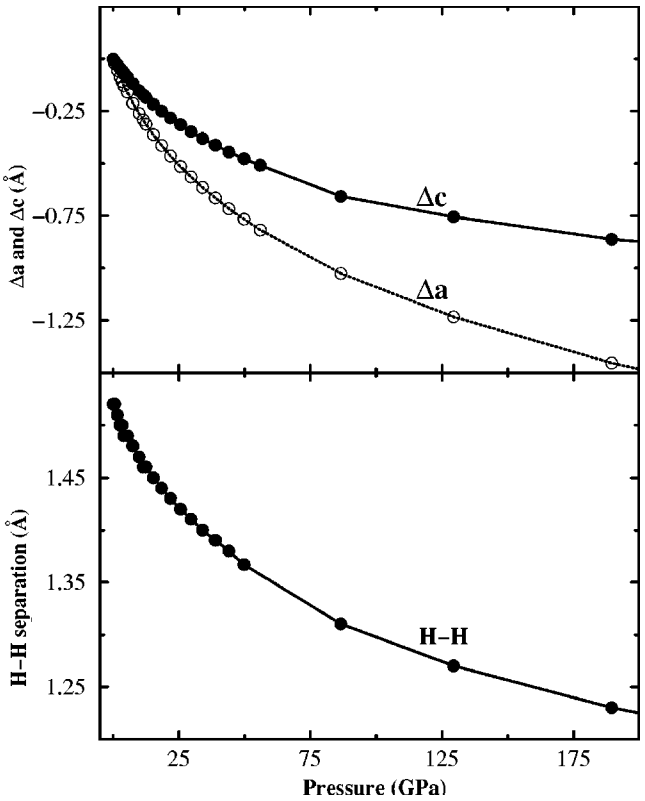

FIG. 8. Shrinkage in lattice parameters (upper panel) and H—H separation (lower panel) for $LaNiInH_{1.333}$ as a function of applied pressure.

accommodated between the hydrogen atoms indicating that they are weakly interacting.

V. CONCLUSION

This study concerns the electronic structure and physical properties of *RT*In and their saturated hydride phases ($RTInH_{1.333}$) investigated by first principle total-energy calculations. The following conclusions are made:

1) The optimized unit-cell volume, c/a, and atomic coordinates are in good agreement with experimental findings for the parent alloy phases. For the $RTInH_{1.333}$ compounds experimental data are only available for T=Ni that indeed show good agreement with the calculated data. The introduction of hydrogen in the parent *RT*In phases causes a highly anisotropic variation in a and c, a large expansion along c (12.4%–20.5%), and a small contraction along a (−0.04 to −5.8%).

2) When one replaces the Ni by Pd or Pt in $RTInH_{1.333}$; the observed H—H separation becomes shortened, which appears to suggest that one with a proper combination of R and T (and perhaps also substitution for In) can obtain phases with even shorter H—H separations.

3) Charge-transfer plots show that charges are transferred from the electron-rich metal atoms (R, T, and In) to hydrogen resulting in an ionic component in the bonding between H and the *RT*In host matrix. ELF analyses show weak metallic-like interactions between the nearest-neighbor hydrogen atoms. The metallic-like bonding with a small ionic contribution between T and H is in turn, taken in support of presence of distinguishable molecular-like H—T—H (TH_2) units in an otherwise metal-matrix jelly.

4) According to charge density and COHP analyses, the direct H—H interaction is weak compared with the T—H interactions. Hence, the shortest distance between the H atoms in $RTInH_{1.333}$ is governed primarily by the polarization of the negative charges on H toward the electropositive R and In atoms.

5) High-pressure simulations show that formation of more H_2-like units in $RTInH_{1.333}$ matrices is not feasible even at ultra-high pressures (up to 400 GPa).

6) The occurrence of very short T—H and unusual H—H separations would at first sight suggest that the $RTInH_{1.333}$ phases belong to the complex hydride family. However, a careful analysis of all facts show that these compounds should be classified as normal metal hydrides.

7) All $RTInH_{1.333}$ phases have nonvanishing density of states at the Fermi level and should accordingly exhibit metallic conductivity.

ACKNOWLEDGMENTS

P.V. and P.R. gratefully acknowledge Professor O.K. Andersen and Professor J. Wills for being allowed to use their computer codes and the Research Council of Norway for financial support. This work has also received support from The Research Council of Norway (Programme for Supercomputing) through a grant of computing time.

*Electronic address: ponniahv@kjemi.uio.no; URL: http://folk.uio.no/ponniahv

[1] P. Ravindran, P. Vajeeston, R. Vidya, A. Kjekshus, and H. Fjellvåg, Phys. Rev. Lett. **89**, 106403 (2002).
[2] P. Vajeeston, P. Ravindran, R. Vidya, A. Kjekshus, H. Fjellvåg, and V. A. Yartys, Phys. Rev. B **67**, 014101 (2003).
[3] K. H. J. Buschow, H. H. Van Mall, P. D. Googwell, and P. S. Rudman, J. Less-Common Met. **29**, 203 (1972).
[4] J. J. Reilly and R. H. Wiswall, Inorg. Chem. **13**, 218 (1974).
[5] N. F. Mott and H. Jones, *The Theory of Metals and Alloys* (Oxford University Press, London, 1936).
[6] M. Yoshida, E. Akiba, Y. Shimojo, Y. Morii, and F. Izumi, J. Alloys Compd. **231**, 755 (1995).
[7] D. G. Westlake, J. Less-Common Met. **103**, 203 (1984).
[8] D. P. Shoemaker and C. B. Shoemaker, J. Less-Common Met. **68**, 43 (1979).
[9] K. Yvon and P. Fischer, in *Hydrogen in Intermetallic Compounds*, edited by L. Schlapbach, Topics in Applied Physics, Vol. 63 (Springer, Berlin, 1988), p. 87.
[10] C. Switendick, Z. Phys. Chem., Neue Folge **117**, 89 (1979).

[11] K. Ghoshray, B. Bandyopadhyay, M. Sen, A. Ghoshray, and N. Chatterjee, Phys. Rev. B **47**, 8277 (1993).
[12] M. Sen, S. Giri, K. Ghoshray, G. Bandyopadhyay, G. Ghoshray, and N. Chatterjee, Solid State Commun. **89**, 327 (1994).
[13] M. Sen, A. Ghoshray, K. Ghoshray, S. Sil, and N. Chatterjee, Phys. Rev. B **53**, 14 345 (1996).
[14] V. A. Yartys, R. V. Denys, B. C. Hauback, H. Fjellvåg, I. I. Bulyk, A. B. Riabov, and Y. M. Kalychak, J. Alloys Compd. **330–332**, 132 (2002).
[15] S. C. Abrahams, A. P. Ginsberg, and K. Knox, Inorg. Chem. **3**, 558 (1964); K. Knox, and A. P. Ginsberg, *ibid.* **3**, 555 (1964).
[16] J. M. Wills and B. R. Cooper, Phys. Rev. B **36**, 3809 (1987); D. L. Price and B. R. Cooper, *ibid.* **39**, 4945 (1989).
[17] J. P. Perdew, in *Electronic Structure of Solids*, edited by P. Ziesche and H. Eschrig (Akademie Verlag, Berlin, 1991) p. 11; J. P. Perdew, K. Burke, and Y. Wang, Phys. Rev. B **54**, 16 533 (1996); J. P. Perdew, K. Burke, and M. Ernzerhof, Phys. Rev. Lett. **77**, 3865 (1996).
[18] L. Hedin and B. I. Lundqvist, J. Phys. C **4**, 2064 (1971).
[19] M. Richter, J. Phys. C **31**, 1017 (1998); C. Ambosch-Draxl, P. Blaha, and K. Schwarz, J. Phys.: Condens. Matter **6**, 2347 (1994); M. Divis, K. Schwarz, P. Blaha, G. Hilscher, H. Michor, and S. Khmelevskyi, Phys. Rev. B **62**, 6774 (2000); http://www.wien2k.at/reg_user/faq/open_core.html
[20] D. J. Chadi and M. L. Cohen, Phys. Rev. B **8**, 5747 (1973).
[21] S. Froyen, Phys. Rev. B **39**, 3168 (1989).
[22] P. E. Blochl, O. Jepsen, and O. K. Andersen, Phys. Rev. B **49**, 16 223 (1994).
[23] P. Vinet, J. Ferrante, J. R. Smith, and J. H. Rose, J. Phys. C **19**, L467 (1986); P. Vinet, J. H. Rose, J. Ferrante, and J. R. Smith, J. Phys.: Condens. Matter **1**, 1941 (1989).
[24] F. Birch, Phys. Rev. **71**, 809 (1947).
[25] F. D. Murnaghan, Proc. Natl. Acad. Sci. U.S.A. **30**, 244 (1944).
[26] O. K. Andersen and O. Jepsen, Phys. Rev. Lett. **53**, 2571 (1984).
[27] U. von Barth and L. Hedin, J. Phys. C **5**, 1629 (1972).
[28] R. Dronskowski and P. E. Blochl, J. Phys. Chem. **97**, 8617 (1993).
[29] G. Krier, O. Jepsen, A. Burkhardt, and O. K. Andersen, *Tight Binding LMTO-ASA Program Version 4.7* (Stuttgart, Germany, 2000).
[30] L. Schlapbach, F. Meli, and A. Zuttel in *Intermetallic Compounds*, Vol. 2, edited by J. H. Westbrook and R. L. Fleischer (Wiley, New York, 1994), p. 475.
[31] P. Villars and L. D. Calvert, *Pearson's Handbook of Crystallographic Data for Intermetallic Phases*, Vol. 3 (American Society for Metals, Materials Park, OH, 1985).
[32] I. I. Bulyk, V. A. Yartys, R. V. Denys, Y. M. Kalychak, and I. R. Harris, J. Alloys Compd. **284**, 256 (1999).
[33] R. D. Shannon, Acta Crystallogr., Sect. A: Cryst. Phys., Diffr., Theor. Gen. Crystallogr. **32**, 751 (1976).
[34] W. M. Mueller, J. P. Blackledge, and G. G. Libowitz, *Metal Hydrides* (Academic Press, NY, 1968).
[35] C. D. Gelatt, A. R. Williams, and V. L. Moruzzi, Phys. Rev. B **27**, 2005 (1983).
[36] Y. Fukai, *The Metal-Hydrogen System; Basic Bulk Properties* (Springer, Berlin, 1993).
[37] M. Gupta and B. Schlapbach, in *Hydrogen in Intermetallic Compounds I*, edited by B. Schlapbach, Topics Appl. Phys., Vol. 63 (Springer, Berlin, 1988) p. 139.
[38] P. Vajeeston, P. Ravindran, R. Vidya, H. Fjellvåg, and A. Kjekshus (unpublished).
[39] A. Savin, A. D. Becke, J. Flad, R. Nesper, H. Preuss, and H. G. von Schnering, Angew. Chem., Int. Ed. Engl. **30**, 409 (1991); A. Savin, O. Jepsen, J. Flad, O. K. Andersen, H. Preuss, and H. G. von Schnering, *ibid.* **31**, 187 (1992).
[40] B. Silvi and A. Savin, Nature (London) **371**, 683 (1994).
[41] A. D. Becke and K. E. Edgecombe, J. Chem. Phys. **92**, 5397 (1990).
[42] L. G. Hector, J. F. Herbst, and T. W. Capehart, J. Alloys Compd. **353**, 74 (2003).
[43] M. Stange, V. A. Yartys, J. P. Mæhlen, and M. Hanfland, J. Alloys Compd. **356–357**, 395 (2003).
[44] K. Yvon, Chimia **52**, 613 (1998).
[45] K. Yvon in *Encyclopedia of Inorganic Chemistry*, edited by R. Bruce King, Vol. 3 (John Wiley & Sons, NY, 1994), p. 1401.